

Coulomb-interaction effects on the electronic structure of radially polarized excitons in nanorings

Z. Barticevic and M. Pacheco

Departamento de Física, Universidad Técnica Federico Santa María, Casilla 110-V, Valparaíso, Chile

J. Simonin and C. R. Proetto

Centro Atómico Bariloche and Instituto Balseiro, 8400 S. C. de Bariloche, Río Negro, Argentina

(Received 21 July 2005; revised manuscript received 7 November 2005; published 12 April 2006)

The electronic structure of radially polarized excitons in structured nanorings is analyzed, with emphasis in the ground-state properties and their dependence under applied magnetic fields perpendicular to the ring plane. The electron-hole Coulomb attraction has been treated rigorously, through numerical diagonalization of the full exciton Hamiltonian in the noninteracting electron-hole pairs basis. Depending on the relative weight of the kinetic energy and Coulomb contributions, the ground-state of polarized excitons has “extended” or “localized” features. In the first case, corresponding to small rings dominated by the kinetic energy, the ground-state shows Aharonov-Bohm (AB) oscillations due to the individual orbits of the building particles of the exciton. In the localized regime, corresponding to large rings dominated by the Coulomb interaction, the only remaining AB oscillations are due to the magnetic flux trapped *between* the electron and hole orbits. This dependence of the exciton, a neutral excitation, on the flux difference confirms this feature as a signature of Coulomb dominated polarized excitons. Analytical approximations are provided in both regimes, which accurately reproduce the numerical results.

DOI: [10.1103/PhysRevB.73.165311](https://doi.org/10.1103/PhysRevB.73.165311)

PACS number(s): 78.67.Bf, 73.21.-b, 73.40.Rw, 78.66.Fd

I. INTRODUCTION

Nanoscale semiconductor structures have been the subject of numerous theoretical and experimental investigations in the last few years. The effects of quantum confinement in these nanosystems strongly modify their electronic and optical properties, offering exciting possibilities for technological applications. Among these, a particular class of structures with annular geometry called nanorings are being intensively investigated after the experimental observation of the AB¹ effect in small metallic rings.^{2–6} With the strong development in the nanofabrication, it is now possible the formation of different types of semiconductor nanorings.⁷ This gives us the exciting opportunity to observe new quantum interference phenomena in magneto-optical experiments.^{8,9} Several theoretical papers have reported studies about the influence of the different geometric-confinement parameters and the presence of impurities on the spectrum in a semiconductor quantum ring in magnetic fields.^{10–13} The effects of an external electric field on the AB oscillations in the energy spectrum of quantum rings have also been reported.¹⁴ Most of the experimental work has been performed on charged excitons in nanorings^{8,9,15,16} and in neutral excitons in type-II quantum dots.¹⁷ The possibility of the observation of the so-called “optical” AB has been an interesting and controversial subject in the recent years.^{18–21} It was predicted that the polarization of a neutral exciton in a quantum ring can originate a magnetic interference effect such that the ground-state of the exciton alternates between states with zero (bright) and non-zero (dark) angular momentum for increasing magnetic field.^{22–25} The finite polarization of the exciton can be obtained by asymmetries in the confinement potentials of the electron and holes or by means of a uniform electric field

applied in the ring plane.²⁶ In the present paper we report a study of the effects of the Coulomb interaction on the electronic structure of excitons in nanorings. We consider radially polarized excitons and we make a detailed analysis of the ground-state properties and its dependence with magnetic fields applied perpendicular to the ring plane. We include rigorously the electron-hole Coulomb interaction and discuss different regimes of excitonic confinement. We also provided analytical approximations which are useful for semiquantitative estimations in well-defined regimes.

II. THE MODEL AND METHOD OF SOLUTION

The effective-mass excitonic Hamiltonian in a quantum-ring structure subject to an external magnetic field parallel to the ring axis, which we take to be the z axis, can be simplified under some suppositions. In the first place, the electron and hole coordinates along the z -direction may be “frozen” at the same in-plane value (say, $z_e = z_h = 0$). This is consistent with the fact that for all the semiconductor quantum rings produced by today’s semiconductor growth techniques, the confinement along the z -direction (usually given by a compositional barrier) is much stronger than the in-plane confinement. This gives rise to a strong quantization along z . In the second place, the radial displacements of the electron and hole may also be frozen at different radial coordinates, R_e and R_h , respectively. This is done by assuming that the effective self-consistent potentials, for electron and for hole, have different radial positions for their respective minima^{28,29} and by realizing that the confinement and its associated energy quantization in the radial direction is usually stronger than in the azimuthal direction, for both of them. These two approximations leads directly to:²³

$$\hat{H}_{exc}(\theta_e, \theta_h) = \hat{H}_{exc}^0(\theta_e, \theta_h) + U_c(\Delta\theta), \quad (1)$$

where

$$\hat{H}_{exc}^{(0)}(\theta_e, \theta_h) = \frac{\hbar^2}{2m_e R_e^2} \left(-i \frac{\partial}{\partial \theta_e} + \frac{\phi_e}{\phi_0} \right)^2 + \frac{\hbar^2}{2m_h R_h^2} \left(i \frac{\partial}{\partial \theta_h} + \frac{\phi_h}{\phi_0} \right)^2, \quad (2)$$

is the sum of the electron and hole kinetic energies, and the Coulomb interaction is given by

$$U_c(\Delta\theta) = - \frac{e^2}{\varepsilon(R_e^2 + R_h^2)^{1/2}} \frac{1}{[1 - r \cos(\Delta\theta)]^{1/2}}. \quad (3)$$

In the above equations $\Delta\theta = \theta_e - \theta_h$, m_e , and m_h are the electron and hole effective masses, (R_e, θ_e) and (R_h, θ_h) are the radial and angular electron and hole polar coordinates, $\phi_e = \pi B R_e^2$, $\phi_h = \pi B R_h^2$ are the magnetic fluxes threading the electron and hole rings, and $\phi_0 = ch/e$ is the flux quantum. $U_c(\Delta\theta)$ describes the Coulomb attraction between the electron and the hole, with ε the dielectric constant of the semiconductor ring material, and the parameter $r = 2(R_e/R_h)/[1 + (R_e/R_h)^2]$ determines the shape and the strength of the Coulomb interaction. For $r \rightarrow 0$ ($R_h \gg R_e$) the Coulomb potential as a function of $\Delta\theta$ is nearly flat, while for $r \rightarrow 1$ ($R_h \approx R_e$), the potential has a pronounced minimum at $\Delta\theta = 0$.

The model defined by Eqs. (1)–(3) is quite appropriate for the calculation of the energy spectrum and angular structure of radially polarized excitons in nanorings. For the study of the photoluminescence response of the system it must be also taken into account the Gaussian-type radial extension of the electron and hole wave functions.²⁷ The presence of a finite radial overlap between both wave functions thus gives a finite interband matrix element.

Even after these simplifications, $\hat{H}_{exc}(\theta_e, \theta_h)$ is not exactly solvable, at least analytically, due to the Coulomb interaction. In consequence, we have used the following direct numerical strategy: Diagonalization of Eq. (1) in the noninteracting electron-hole pairs basis generated by the eigenstates of $\hat{H}_{exc}^0(\theta_e, \theta_h)$,

$$\hat{H}_{exc}^0(\theta_e, \theta_h) \psi_{\ell_e, \ell_h}^0(\theta_e, \theta_h) = E_{\ell_e, \ell_h}^{(0)} \psi_{\ell_e, \ell_h}^0(\theta_e, \theta_h), \quad (4)$$

where

$$\psi_{\ell_e, \ell_h}^0(\theta_e, \theta_h) = \frac{1}{(2\pi)} e^{i\theta_e \ell_e} e^{i\theta_h \ell_h}, \quad (5)$$

and

$$E_{\ell_e, \ell_h}^{(0)}(B) = \frac{\hbar^2}{2m_e R_e^2} \left(\ell_e + \frac{\phi_e}{\phi_0} \right)^2 + \frac{\hbar^2}{2m_h R_h^2} \left(\ell_h - \frac{\phi_h}{\phi_0} \right)^2, \quad (6)$$

where ℓ_e and $\ell_h (= 0, \pm 1, \pm 2, \dots)$ are the electron and hole angular momentum quantum numbers, respectively. The noninteracting eigenstates of Eq. (5) can also be written in terms of $\Delta\theta$ and a new angular variable, given by

$$\theta_0 = (I_e \theta_e + I_h \theta_h)/I, \quad (7)$$

here $I_e = m_e R_e^2$, $I_h = m_h R_h^2$, and $I = I_e + I_h$ are the electron, hole, and total moments of inertia, respectively. θ_0 is then a gen-

eralized angular “center of mass” (c.m.) coordinate, and describes the translation of the *whole* exciton around the ring, while $\Delta\theta$ describes the internal (relative) exciton dynamics. Replacing in Eq. (5), we obtain,

$$\psi_{\ell_e, \ell_h}^0(\theta_0, \Delta\theta) = \frac{1}{2\pi} e^{i\theta_0(\ell_e + \ell_h)} e^{i\Delta\theta(\ell_e I_e - \ell_h I_h)/I}. \quad (8)$$

The important point to note now is that as the Coulomb interaction only depends on $\Delta\theta$, the total angular momentum of the polarized exciton $L \equiv \ell_e + \ell_h$ remains a good quantum number even in the interacting regime; this is a consequence of the azimuthal rotational symmetry of the structured rings. Thus, the Hamiltonian matrix generated in the basis of Eq. (5) is block-diagonal, with each block corresponding to a given $L (= 0, \pm 1, \pm 2, \dots)$. The numerical diagonalization of each block provides the eigenvalues and eigenstates of \hat{H}_{exc} , which we denote by $E_{L,n}(B)$ and $\varphi_{L,n}(\theta_0, \Delta\theta)$, respectively, with $n = 1, 2, \dots$. To obtain accurate exciton energies and wave functions from the basis generated from Eq. (5), we truncate the basis by choosing an adequate set of quantum numbers ℓ_e and $\ell_h (= -\ell_e + L)$ in each L sub-space. This set is chosen starting from the couple ℓ_e, ℓ_h which correspond to the magnetic-field dependent noninteracting ground-state energy. The size of the basis is chosen large enough such that the results do not depend on it. The only nontrivial point of this calculation scheme is the numerical evaluation of the matrix elements of $U_c(\Delta\theta)$ between the noninteracting eigenstates of Eq. (5). While formally these matrix elements can be written in terms of the so-called toroidal functions,²⁵ for its practical and accurate evaluation we have found the direct numerical integration over the one-dimensional variable $\Delta\theta$ more convenient. Also, considering the easiness of its direct numerical evaluation, we do not recommend its evaluation through the large-size ring approximation,²⁵ as we have found that it leads to some over-estimation of the exciton binding energy.

III. RESULTS

All the numerical results to be discussed below were obtained with material parameters appropriate for GaAs, that is: $m_e = 0.067 m_0$, $m_h = 0.268 m_0$, and $\varepsilon = 12.5$, with m_0 being the bare electron mass. The effective Bohr radius for the electron (a_0^*) is then equal to 98.7 Å. Also, we have assumed that $R_e \leq R_h$.

Before we proceed with the results a brief note on terminology is worth discussing. In principle, the numerical diagonalization of the exciton Hamiltonian results in a large number of eigenvalues, for each structured ring and magnetic field value. Our analysis, however, will be mainly concentrated on the *lowest* of these eigenvalues, the ground-state exciton. This ground-state exciton will be characterized in turn as belonging to the weak-interacting (WI) regime, or to the strong-interacting (SI) regime (see below). Excited exciton states will be more properly considered as electron-hole pairs.

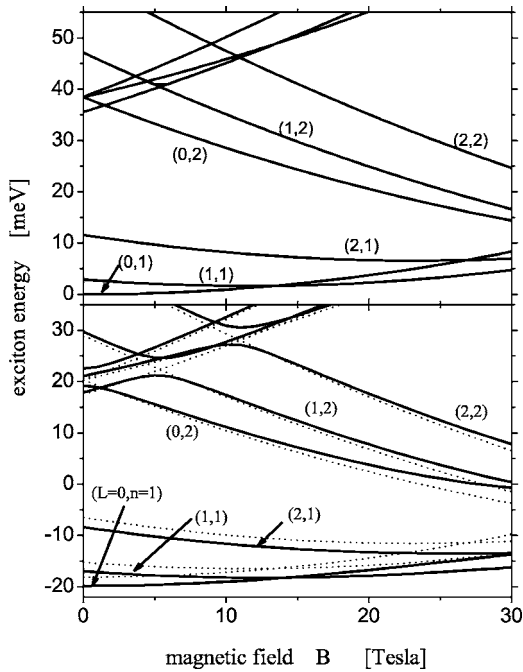


FIG. 1. Exciton energy vs magnetic field, for a ring with $R_e = 40 \text{ \AA}$, $R_h = 70 \text{ \AA}$. Only states with total angular momentum $L = 0, 1$, and 2 are plotted, and for each of these, the three lowest ones. Upper panel, noninteracting case. Lower panel, interacting case: Perturbative expression (dotted lines) and numerical results (full lines).

A. Weak interacting regime

In this regime, corresponding to structured rings of small size, the dominant contributions to $\hat{H}_{exc}(\theta_e, \theta_h)$ are the kinetic energy terms, with the Coulomb interaction acting as a small modification to the noninteracting results. Including accordingly $U_c(\Delta\theta)$ in a perturbative way, we obtain

$$E_{\ell_e, \ell_h}^{(1)}(B) = E_{\ell_e, \ell_h}^{(0)}(B) - \frac{2e^2}{\pi\epsilon(R_e + R_h)} K \left[\frac{4R_e R_h}{(R_e + R_h)^2} \right], \quad (9)$$

with $K(x)$ being the complete elliptic integral of the first kind.³⁰ The second term on the r.h.s. of Eq. (9) corresponds to the matrix element $U_c(m) \equiv \langle \psi_{\ell_e - m, \ell_h + m}^0 | U_c | \psi_{\ell_e, \ell_h}^0 \rangle$, with $m=0$. This diagonal matrix element is the *same* for all couples of (ℓ_e, ℓ_h) noninteracting electron-hole quantum numbers. Besides, in this regime, $|U_c(0)| \gg |U_c(m \neq 0)|$, which supports the perturbative expression Eq. (9). According to this result, the exciton energy spectrum in the WI regime is the same as the noninteracting spectrum, but shifted rigidly by a negative constant.

We show in Fig. 1 the energy spectrum for a radial polarized exciton (RPE) in the WI regime, corresponding to a ring with $R_e = 40 \text{ \AA}$ and $R_h = 70 \text{ \AA}$. The top panel corresponds to the noninteracting spectrum, the lower panel to the interacting spectrum calculated exactly (numerically), and as given by the perturbative expression of Eq. (9). As can be seen from the results in the lower panel, the perturbative approximation nicely reproduces the main features of the numerical result, shifting the noninteracting spectrum towards negative

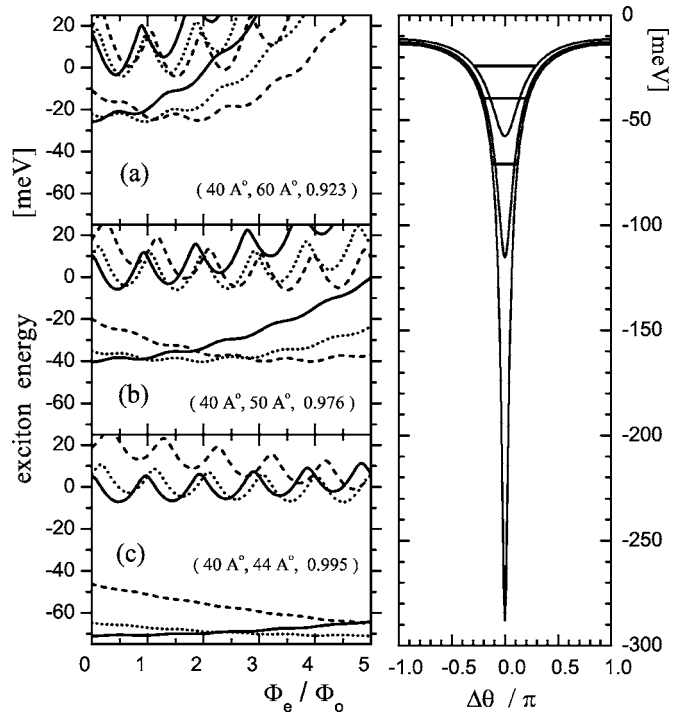


FIG. 2. Left panel, exciton energy spectrum vs electron magnetic flux, for three structured rings. Only the first low-lying states with $L=0$ (full lines), $L=1$ (dotted lines), and $L=2$ (dashed lines) are shown. Right panel: Coulomb attractive potential $U_c(\Delta\theta)$ for the three structured rings of the left panel, the horizontal bars in them correspond to the lowest lying state (see text).

energies by about 18 meV. It is interesting to note that the approximation works better for excited than for low-lying states. This is natural, as if the kinetic energy increases at constant Coulomb correction, the accuracy of the perturbative approach should increase. Beyond this simple first-order estimation are the several anticrossings which appear in the numerical results when two states with the same L approach each other as function of B .

The parameters used in Fig. 1 are similar to those used in the noninteracting case studied in Fig. 2 of Ref. 22. There it is shown that the $L=0$ (bright) and $L \neq 0$ (dark) exciton alternate as ground-state, as a function of the applied magnetic field. However, then the Coulomb interaction is included in the calculations we found that this “blinking” behavior of the exciton is precluded. In our case, once the $L=0$ ground-state crosses the $L=1$ ground-state, it does not become again the ground-state.

B. From the weak to the strong interacting regime

By approaching R_e and R_h to each other ($r \rightarrow 1$), the Coulomb attraction between the hole and the electron is increasingly more important than the kinetic energy terms. We show this crossover in Fig. 2, where we display the RPE spectrum for decreasing values of R_h , keeping $R_e = 40 \text{ \AA}$. The more noticeable feature of these results is the progressive appearance of a “gap” among the low-lying and the excited states, for each L sub-space. Moving from top to bottom (left

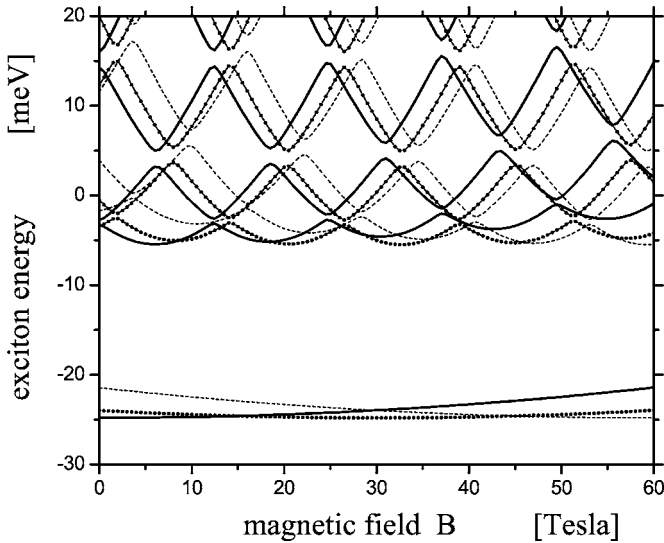


FIG. 3. Exciton energy vs magnetic field for a ring with $R_e = 100 \text{ \AA}$, $R_h = 120 \text{ \AA}$. Only states with total angular momentum $L = 0$ (full lines), 1 (dotted lines), and 2 (dashed lines) are plotted.

panel), the modification of the spectrum consist mainly in a progressive “deepening” of the given L low-lying state towards negative energies, while the excited states remain at energies close to zero. The right panel in Fig. 2 corresponds to $U_c(\Delta\theta)$, with the deeper one corresponding to $R_h = 44 \text{ \AA}$ ($r = 0.995$), and the shallow one to $R_h = 60 \text{ \AA}$ ($r = 0.923$). The straight horizontal lines denote the position of the lowest-lying states of the left panel (discounting the c.m. motion) for each size of the structured ring; once the kinetic energy of the c.m. motion has been subtracted the remaining energy becomes essentially independent of L and B (see below). With this information at hand the meaning of the three split low-lying states of Fig. 2(c) is clear: They correspond to localized exciton states, whose wave function (internal component) is strongly localized around $|\Delta\theta| \approx 0$. This must be contrasted with the noninteracting exciton wave function of Eq. (8), whose internal component is uniformly distributed along its allowed values ($|\Delta\theta| \leq \pi$). Physically, this localization of the ground-state exciton wave function is driven by the attractive Coulomb interaction, which for $r \rightarrow 1$ is able of keep the electron and hole as close as possible, losing kinetic energy but gaining Coulomb energy. An interesting feature of these results is that as more localized is a state, less dependence on the magnetic flux trapped by its individual components it shows. This issue will be discussed in detail in the next sub-section. We emphasize that the characterization of a state as extended or localized refers only to the internal component of the total exciton wave function. The c.m. component is always extended, as corresponds to a system with azimuthal rotational symmetry.

C. Strong interacting regime

Increasing further the structured ring size, the system is driven to the SI regime, where the electron and hole strongly interact. Figure 3, corresponding to a ring with $R_e = 100 \text{ \AA}$, $R_h = 120 \text{ \AA}$, displays clearly one set of localized $L (=0, 1, \text{ and } 2)$

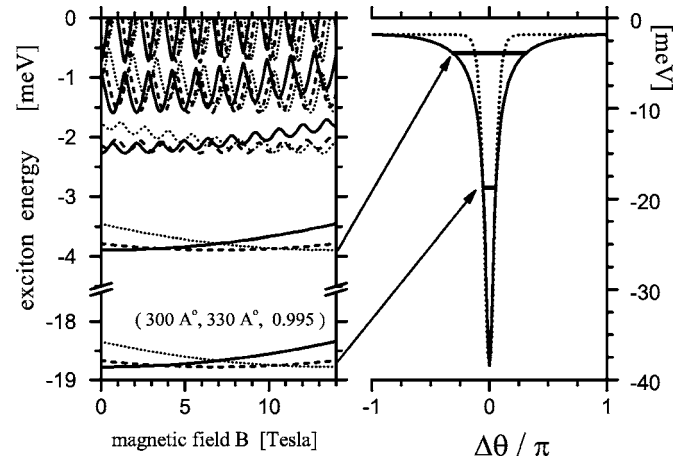


FIG. 4. Left panel, exciton energy spectrum vs magnetic field for a ring with $R_e = 300 \text{ \AA}$, $R_h = 330 \text{ \AA}$. Only the first low-lying states with $L = 0$ (full lines), 1 (dashed lines), and 2 (dotted lines) are shown. Right panel: Coulomb attractive potential $U_c(\Delta\theta)$ (solid line), $V_c(\Delta\theta)$ (dashed line), and discrete energy levels (straight lines). Note the cut in the vertical axis of the left panel.

2) ground-states at negative energies, plus a bunch of closely energy spaced and strongly magnetic field dependent states at positive or close to zero energies. Figure 4 corresponds to an even larger structured ring, with the new feature of having *two* localized sets of states at negative energies, instead of one. The new localized set corresponds to the first-excited state of each L .

An important feature of Figs. 3 and 4, is the presence of a characteristic energy (negative but close to zero), above of which all states are extended. This energy is just $U_c(\Delta\theta = \pm\pi) = -e^2/\epsilon(R_e + R_h)$, corresponding to the minimum strength that the Coulomb potential can take in the constrained-ring geometry, and associated to the maximum possible interparticle distance. For the ring of Fig. 2(c), $U_c(\Delta\theta = \pm\pi) \approx -13.71 \text{ meV}$, for the ring of Fig. 3 $U_c(\Delta\theta = \pm\pi) \approx -5.23 \text{ meV}$, and about -1.83 meV for the ring of Fig. 4. Conversely, all states below that energy are localized and their corresponding energies show a very weak dependence on L and B , as we will discuss later.

To analyze properly the results of the SI regime, it is useful to rewrite $\hat{H}_{exc}(\theta_e, \theta_h)$ in term of the variables $\theta_0, \Delta\theta$:

$$\hat{H}_{exc}(\theta_e, \theta_h) = \hat{H}_{exc}(\theta_0, \Delta\theta) = \hat{H}_{c.m.}(\theta_0) + \hat{H}_{int}(\Delta\theta), \quad (10)$$

with

$$\hat{H}_{c.m.}(\theta_0) = \frac{\hbar^2}{2I} \left(-i \frac{\partial}{\partial \theta_0} + \frac{\phi_{c.m.}}{\phi_0} \right)^2 \quad (11)$$

and

$$\hat{H}_{int}(\Delta\theta) = \frac{\hbar^2}{2I_{int}} \left(-i \frac{\partial}{\partial (\Delta\theta)} + \frac{\phi_{int}}{\phi_0} \right)^2 + U_c(\Delta\theta). \quad (12)$$

The main achievement of this transformation is the *exact* decoupling of the translational (θ_0) and relative coordinates ($\Delta\theta$).²³ In the equation above, $\phi_{c.m.} = \pi(R_e^2 - R_h^2)B$, $I_{int} = I_e I_h / I$, and $\phi_{int} = \pi I_{int} B / \mu$, with $\mu = m_e m_h / (m_e + m_h)$.

Being $\hat{H}_{exc}(\theta_0, \Delta\theta)$ the sum of the c.m. and internal contributions, the corresponding eigenvalues are given by

$$E_{L,n}(B) = \frac{\hbar^2}{2I} \left(L + \frac{\phi_{c.m.}}{\phi_0} \right)^2 + \varepsilon_{L,n}(B) \quad (13)$$

and

$$\varphi_{L,n}(\theta_0, \Delta\theta) = g_L(\theta_0) h_{L,n}(\Delta\theta), \quad (14)$$

with $g_L(\theta_0)$ being eigenfunctions of $\hat{H}_{c.m.}(\theta_0)$ and $\varepsilon_{L,n}(B)$ and $h_{L,n}(\Delta\theta)$ the eigenvalues and eigenfunctions of $\hat{H}_{int}(\Delta\theta)$, respectively. While the solution of $\hat{H}_{c.m.}(\theta_0)$ is immediate, the solution of $\hat{H}_{int}(\Delta\theta)$ is not, due to its combined magnetic and Coulomb contributions, and the cumbersome cyclic boundary-conditions for its associated eigenfunctions. Some insight can be obtained, however, through the following gauge transformation of the internal component of the total exciton wave function,

$$h_{L,n}(\Delta\theta) = e^{-i\Delta\theta\phi_{int}/\phi_0} f_{L,n}(\Delta\theta). \quad (15)$$

The boundary conditions for the total exciton wave function are easily established in terms of the angular coordinates θ_e, θ_h : $\varphi_{L,n}(\theta_e, \theta_h) = \varphi_{L,n}(\theta_e + 2\pi, \theta_h) = \varphi_{L,n}(\theta_e, \theta_h + 2\pi) = \varphi_{L,n}(\theta_e + 2\pi, \theta_h + 2\pi)$. From these boundary conditions, it could be easily derived an equivalent set of boundary conditions in terms of θ_0 and $\Delta\theta$: $\varphi_{L,n}(\theta_0, \Delta\theta) = \varphi_{L,n}(\theta_0 + 2\pi I_e/I, \Delta\theta + 2\pi) = \varphi_{L,n}(\theta_0 + 2\pi I_h/I, \Delta\theta - 2\pi) = \varphi_{L,n}(\theta_0 + 2\pi, \Delta\theta)$. Finally, using Eqs. (14) and (15), the boundary conditions for the individual components of $\varphi_{L,n}(\theta_0, \Delta\theta)$ are $g(\theta_0) = g(\theta_0 + 2\pi)$, and

$$f_{L,n}(\Delta\theta) = \exp \left[2\pi i \left(\frac{I_e L}{I} + \frac{\phi_{int}}{\phi_0} \right) \right] f_{L,n}(\Delta\theta + 2\pi), \quad (16a)$$

$$f_{L,n}(\Delta\theta) = \exp \left[2\pi i \left(\frac{I_h L}{I} - \frac{\phi_{int}}{\phi_0} \right) \right] f_{L,n}(\Delta\theta - 2\pi). \quad (16b)$$

Replacing the ansatz of Eq. (15) in $\hat{H}_{int}(\Delta\theta) h_{L,n}(\Delta\theta) = \varepsilon_{L,n}(B) h_{L,n}(\Delta\theta)$, we derive an effective equation that defines $f_{L,n}(\Delta\theta)$; this equation is:

$$-\frac{\hbar^2}{2I_{int}} \frac{\partial^2 f_{L,n}(\Delta\theta)}{\partial(\Delta\theta)^2} + U_c(\Delta\theta) f_{L,n}(\Delta\theta) = \varepsilon_{L,n}(B) f_{L,n}(\Delta\theta). \quad (17)$$

The wave function $f_{L,n}(\Delta\theta)$ satisfies then a magnetic-field independent one-dimensional Schrödinger-type equation. The magnetic field dependence of $\varepsilon_{L,n}(B)$ is hidden now in the boundary conditions for $f_{L,n}(\Delta\theta)$.

Summarizing, $f_{L,n}(\Delta\theta)$ must satisfy the Schrödinger-type Eq. (17), plus the magnetic-field dependent boundary conditions of Eq. (16). Now, and this is the whole point, if the internal wave function $f_{L,n}(\Delta\theta)$ is strongly localized around $\Delta\theta \approx 0$, it makes no difference if we replace the complicated requirement of Eq. (16) by the ‘‘isolated well’’ boundary condition $f_{L,n}(|\Delta\theta| \geq 1) \rightarrow 0$. Proceeding this way, the eigenval-

ues $\varepsilon_{L,n}$ become L and magnetic-field independent, as in this regime the internal Hamiltonian and the boundary condition are *both*, L and magnetic-field independent. The approximation works better the more localized is the state, and can be sought as related to the tight-binding approximation employed in the calculation of the band-structure of crystalline solids.³¹ In this last case, and for an atomic orbital strongly localized on the scale of the lattice parameter, it makes no difference if one uses the rigorous boundary condition imposed by the Bloch theorem or the ‘‘isolated atom’’ boundary condition. In both cases, the rigorous and the approximated calculation gives essentially the same result: A discrete level just at the energy of the atomic orbital of the isolated atom.

Accordingly, in this regime all the magnetic field dependence of the exciton energy comes essentially from the c.m. contribution. Thus, one can estimate the crossing points for exciton states with different total angular momentum such as $L \rightarrow L+M$ from the condition $E_{L,n}(B) = E_{L+M,n}(B)$, neglecting the L and B dependence of $\varepsilon_{L,n}(B)$. Using Eq. (13), we obtain thus for the crossing magnetic fields,

$$B(L \rightarrow L+M) = \frac{\phi_0}{\pi(R_h^2 - R_e^2)} \left(L + \frac{M}{2} \right). \quad (18)$$

It is interesting to note, in this regime, the strong sensitivity of the crossing magnetic-fields to the difference between R_e and R_h . In particular, the optically active (bright) exciton with $L=0$ could be stabilized at larger magnetic fields by just moving to narrower structured rings. Using Eq. (18) for the low-lying states of Figs. 3 and 4, we obtain for the ring of Fig. 3 that $B(0 \rightarrow 1) \approx 14.69$ T, and $B(0 \rightarrow 2) \approx 29.92$ T. Proceeding in the same way with the ring of Fig. 4, we obtain $B(0 \rightarrow 1) \approx 3.48$ T, $B(0 \rightarrow 2) \approx 6.97$ T, and $B(1 \rightarrow 2) \approx 10.45$ T. The good agreement between these estimations and the exact (numerical) results, confirms the hypothesis of the L and magnetic-field independence of $\varepsilon_{L,n}(B)$. It is also worth noting that the crossing of the two sets of low-lying states ($n=1,2$) in Fig. 4 takes place at the same crossing magnetic fields, as one expects if Eq. (18) is valid.

The exciton energies $E_{L,n}(B)$ could be straight forwardly calculated from Eq. (13), once $\varepsilon_{L,n}(B)$ is known. For the localized regime discussed above we provide in the Appendix an analytic (approximated) solution to the problem posed by the corresponding Eq. (17), which is useful for qualitative and semiquantitative estimations of $E_{L,n}(B)$. For instance, Eqs. (A2) and (A3) provide two useful estimations of ε_n (the L and B independent eigenvalues), and the number of bound localized states, respectively. It is interesting to note that this approximated analytical analysis *always* predicted the existence of a localized state. This is in agreement with the output of the much elaborated numerical results. It is worth mentioning that the naive application of the harmonic approximation does not work for the potential of Fig. 4. The reason for that is that $U_c(\Delta\theta)$ is extremely deep and narrow (on the scale $-\pi \leq \Delta\theta \leq \pi$). In consequence, approximating it by an harmonic term in the bottom region, results in such a narrow parabolic potential that the ground-state energy of the corresponding harmonic oscillator (zero-point energy) is well above the ‘‘continuum’’ limit given by $U_c(\Delta\theta = \pm\pi)$. In

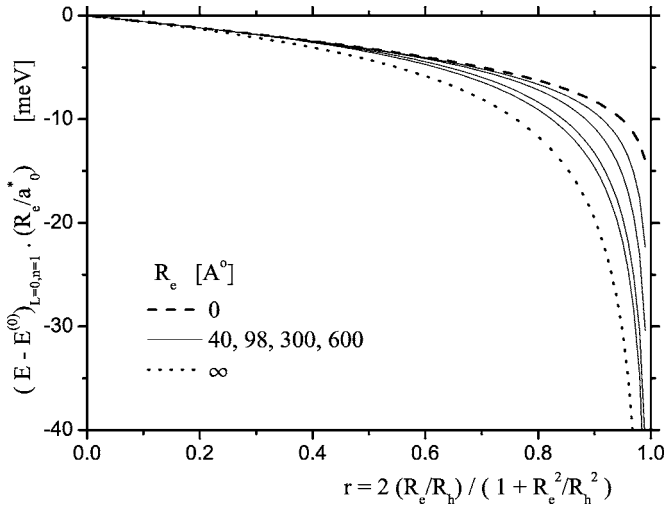


FIG. 5. Coulomb contribution to the ground-state energy, scaled by R_e/a_0^* , at zero magnetic field and rings of several sizes. From top to bottom, $R_e \rightarrow 0$, $R_e = 40 \text{ \AA}$, 98.7 \AA (a_0^*), 600 \AA , and $R_e \rightarrow \infty$.

other words, the harmonic approximation gives no bound-states for the ground-state exciton for this structured ring, while the exact calculation yields two bound-states.

We display in Fig. 5 the Coulomb contribution to the $L = 0$, $n = 1$ radial polarized exciton energy at zero magnetic field and for a set of structured rings of different sizes, scaled by R_e/a_0^* . This contribution has been numerically evaluated from the difference between the interacting and noninteracting ground-state energies, for each ring. The top curve corresponds to the Coulomb perturbative correction of Eq. (9), which could be rewritten as

$$[E_{\ell_e, \ell_h}^{(1)}(B) - E_{\ell_e, \ell_h}^{(0)}(B)] \left(\frac{R_e}{a_0^*} \right) = - \frac{2e^2/a_0^*}{\pi\epsilon(1 + R_h/R_e)} K \left[\frac{4R_h/R_e}{(1 + R_h/R_e)^2} \right]. \quad (19)$$

Note that scaled this way the contributions for different R_e 's all collapse to a single curve. For R_h approaching R_e from above, the argument of the elliptic function tends to one and has a logarithmic divergence.³⁰ The curve at the bottom corresponds to $U_c(\Delta\theta=0)$, scaled with the same factor R_e/a_0^* . Similar to the contribution of Eq. (19), $R_e U_c(\Delta\theta=0)/a_0^*$ collapses to a single curve for all values of R_e 's. In this case, for $R_h/R_e \rightarrow 1$, the divergence is of the type $(R_h - R_e)^{-1}$. The four remaining intermediate curves, correspond from top to bottom to $R_e = 40 \text{ \AA}$, $R_e = a_0^*$, $R_e = 300 \text{ \AA}$, and $R_e = 600 \text{ \AA}$. They have been obtained from the numerical results. The result of Eq. (19) could be considered as giving the limiting value of the Coulomb contribution in the WI regime of $R_e \rightarrow 0$. This explains why the closest curve to this one corresponds to the smallest considered rings, $R_e = 40 \text{ \AA}$. In a similar venue, the curve corresponding to $U_c(\Delta\theta=0)$ could be considered as providing the limiting value of the Coulomb contribution when $R_e \rightarrow \infty$, i.e., well inside of the SI regime. In this ex-

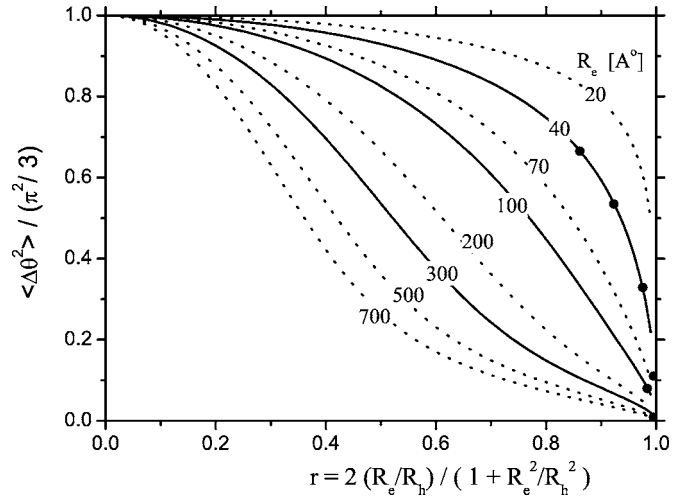


FIG. 6. Expectation value of $\Delta\theta^2$ in the ground state at zero magnetic field, for several ring sizes. The dots on the curves with full lines correspond to the particular ring sizes presented in the previous figures.

treme limit, the exciton behaves as a *classical* particle, its energy given by the minimum of the Coulomb potential at $\Delta\theta=0$. This explains why the curves for increasing values of R_e progressively approach this limiting value.

As an accurate way of characterizing the radial polarized excitons in structured rings we have also calculated the expectation value of $\Delta\theta^2$, in the ground state of the system at zero magnetic field. The results are presented in Fig. 6. In general,

$$\langle (\Delta\theta)^n \rangle \equiv \int_{-\pi}^{\pi} d(\Delta\theta) (\Delta\theta)^n |h(\Delta\theta)|^2, \quad (20)$$

with $h(\Delta\theta)$ the ground state of $\hat{H}_{int}(\Delta\theta)$. As a useful limit, we can evaluate Eq. (20) using the noninteracting zero-field ground-state eigenstate of Eq. (14), which fulfills the normalization condition $|h(\Delta\theta)|^2 = 1/2\pi$. Replacing this in Eq. (20), we obtain

$$\langle \Delta\theta^n \rangle = \frac{\pi^{n+1}}{2\pi(n+1)} [1 - (-1)^{n+1}]. \quad (21)$$

This yields $\langle \Delta\theta \rangle = 0$ and $\langle \Delta\theta^2 \rangle = \pi^2/3$. Consequently, we have plotted $\langle \Delta\theta^2 \rangle / (\pi^2/3)$ in Fig. 6, versus r . When the value of this magnitude is close to 1 we can characterize the ground state of the RPE as extended. Conversely, if $\langle \Delta\theta^2 \rangle / (\pi^2/3) \ll 1$, the ground state is localized. The discrete points on the curves correspond to the structured rings studied in this paper. The utility of this figure lies in the fact that given an arbitrary ring, with the only information of its geometrical dimensions, it is possible to obtain immediately a qualitative characterization of its ground state as extended or localized. It is interesting to note that for intermediate values of r ($r \approx 0.5$), structured rings with the same aspect ratio R_e/R_h could be either in the WI regime ($R_e = 20 \text{ \AA}$), or in the SI regime ($R_e = 700 \text{ \AA}$). For small ($r \approx 0$) or large ($r \approx 1$) val-

ues of r , all rings are either in the WI or in the SI regime, respectively.

It is also important to note that the larger the ring size (as given by R_e), the smaller should be the ratio R_e/R_h in order to achieve the crossover from the SI regime to the WI regime. This is the essential reason why we characterize SI excitons as mainly corresponding to large size rings and WI excitons as corresponding to small size rings.

IV. CONCLUSIONS

We provide an accurate description of the electronic properties of excitons in structured rings, concentrating mainly on the exciton ground states, and their response to magnetic fields applied perpendicular to the ring plane. Our numerical method allows a straightforward and precise calculation of ground-state energy magnitudes for any size of the ring, magnetic field strength, and material value parameters.

We have found that the ground state of polarized excitons can be well characterized in two extreme regimes: (i) The weak interacting regime, where the electron and hole kinetic energies are larger than the Coulomb interaction, and (ii) the strong interacting regime, where the exciton ground-state properties are dominated by the Coulomb electron-hole attraction.

For the weak interacting regime we have provided an analytical approximation. According to this, the weakly interacting excitonic spectrum could be obtained by shifting rigidly the noninteracting spectrum by a negative constant. The constant depends only on the size of the structured rings, but is state-independent. The ground-state exciton WI shows discernible Aharonov-Bohm oscillations with the magnetic field. In this regime it has been predicted²³ the alternate of “bright” ($L=0$) and “dark” ($L \neq 0$) exciton ground-states as a function of the magnetic field. However, for GaAs material parameters, we have found that the rigorous inclusion of the Coulomb interaction removes such effect, and once the $L=0$ ground state crosses with the $L=1$ ground state, it does not become again the ground state.

The ground state in the strong interacting regime depends on the magnetic field only through the phase accumulated by the c.m. angular coordinate, which represents the translation as a whole of the polarized exciton. On the other side, the relative angular coordinate, that describes the internal dynamics of the polarized exciton, remains essentially frozen around zero. We have provided also an analytical approximation for this regime.

We have provided a kind of “phase-diagram” for polarized excitons in GaAs nanorings (Fig. 6), which with the only input of the ring geometrical aspect ratio allows an immediate characterization of the corresponding exciton as localized or extended. Both types of excitons have a very different response under the application of perpendicular magnetic fields.

We have found almost invariably, the simultaneous presence of localized and extended states. This is somewhat similar to the findings of Ref. 14, that have shown a similar excitonic spectrum for the case of a ring with *electric* and magnetic fields applied along and perpendicular to the ring

plane, respectively, in *absence* of Coulomb interaction effects. The rotational and internal structure of the exciton, however, are completely different. In the situation of Ref. 14, the localized states are induced by the applied electric field, that pushes and localizes the electron and hole to opposite sides of the ring. Using our notation and terminology, this kind of exciton has both, the rotational and internal degree of freedom frozen, with θ_0 fixed by the electric field direction, and $|\Delta\theta| \approx \pi$. In our case, the localized states correspond to a tightly bound electron-hole pair, whose relative coordinate is essentially frozen at zero, but whose c.m. coordinate rotates freely around the structured ring.

Note added in proof. After the submission we became aware of a preprint of Dias Da Silva *et al.*²⁵ on magneto-excitons in quantum rings. They study interaction and radial polarization effects on the excitonic absorption spectrum using the model of unidimensional concentric rings. For the strong interacting regime our results are essentially analogous to those of Ref. 25. We coincide that in this regime the lowest optically active state is suppressed for certain structure-dependent critical magnetic field values, whereas the AB effect is manifested through magnetic-field oscillating excited states. However, in the weak-interacting regime we have no evidence in our calculations of a magnetic-field oscillating (bright-dark) ground-state. We believe that this discrepancy is originated in the way they characterize the different interacting regimes: They just take a value of the dielectric constant larger by a factor of ten in the weak-interacting regime. We also have some numerical discrepancies with the results of Ref. 25, which we attribute to their use of an approximate expression for the matrix elements of the Coulomb electron-hole interaction.

ACKNOWLEDGMENTS

Z.B. and M.P. are thankful for the financial support received from Milenio ICM P02-054-F and FONDECYT under Grant Nos. 1050521 and 7020839. J.S. and C.R.P., fellows of CONICET, acknowledge partial financial support from CONICET (Argentina) under Grant No. PIP 02753/00.

APPENDIX: ANALYTICAL APPROACH FOR THE LOCALIZED REGIME

We provide in this Appendix an analytic (approximated) solution to the problem posed by the corresponding Eq. (17), which is useful for qualitative estimations of $E_{L,n}(B)$ in the localized regime. That is, neglecting the dependence of $\varepsilon_{L,n}(B)$ on L and B ; these approximated eigenvalues will be denoted by ε_n . With this aim, we have found that $U_c(\Delta\theta)$ is well approximated by

$$U_c(\Delta\theta) \simeq V_c(\Delta\theta) = -\frac{e^2}{\varepsilon} \frac{1}{|R_e - R_h|} - \frac{V_0}{\cosh(\alpha\Delta\theta)}, \quad (\text{A1})$$

where $V_0 = e^2(1/|R_e - R_h| - 1/|R_e + R_h|)/\varepsilon > 0$, and α is a dimensionless parameter to be determined later. The advantage

of $V_c(\Delta\theta)$ over $U_c(\Delta\theta)$ is that its exact analytical solution is known.³² The eigenvalues associated with the bound solutions are given by

$$\varepsilon_n = \frac{\alpha^2 \hbar^2}{8I_{int}} \left[1 - 2n + \left(1 + \frac{8\mu V_0}{\alpha^2 \hbar^2} \right)^{1/2} \right]^2, \quad (\text{A2})$$

while the eigenfunctions are given in terms of the hypergeometric function.³² It should be noted that Eq. (A2) *always* provided a bound state, corresponding to $n=1$. The number of bound states is, however, finite and given by the condition

$$n_{max} < \frac{1}{2} \left[1 + \left(1 + \frac{8\mu V_0}{\alpha^2 \hbar^2} \right)^{1/2} \right]. \quad (\text{A3})$$

In Eq. (A2), everything is known, except α . In our case, as we have from our full diagonalization scheme the exact value of ε_1 , we have adopted the criteria of choosing α such that it reproduces exactly the numerical value of ε_1 , through Eq. (A2). This produces the value $\alpha=5.458$ for the structured ring of Fig. 4, and the $V_c(\Delta\theta)$ shown as a dashed line in the right panel. This “optimum” choice of α is reflected in the fact that $U_c(\Delta\theta)$ and $V_c(\Delta\theta)$ are identical right at the energy where ε_1 falls. We have checked, however, that the value of ε_1 is not sensitive to the precise value of α and that any other reasonable criteria for its determination [least-square fitting of $U_c(\Delta\theta)$, etc.], works as well as our optimum fitting.

-
- ¹Y. Aharonov and D. Bohm, *Phys. Rev.* **115**, 485 (1959).
²M. Büttiker, Y. Imry, and R. Landauer, *Phys. Lett.* **96A**, 365 (1983).
³V. Chandrasekhar, R. A. Webb, M. J. Brady, M. B. Ketchen, W. J. Gallagher, and A. Kleinsasser, *Phys. Rev. Lett.* **67**, 3578 (1991).
⁴D. Mailly, C. Chapelier, and A. Benoit, *Phys. Rev. Lett.* **70**, 2020 (1993).
⁵U. Keyser, S. Borck, R. J. Haug, M. Bichler, G. Abstreiter, and W. Wegscheider, *Semicond. Sci. Technol.* **17**, 122 (2002).
⁶A. Tonomura, N. Osakabe, T. Matsuda, T. Kawasaki, J. Endo, S. Yano, and H. Yamada, *Phys. Rev. Lett.* **56**, 792 (1986).
⁷B. C. Lee, O. Voskoboynikov, and C. P. Lee, *Physica E (Amsterdam)* **24**, 87 (2004).
⁸M. Bayer, M. Korkusinski, P. Hawrylak, T. Gutbrod, M. Michel, and A. Forchel, *Phys. Rev. Lett.* **90**, 186801 (2003).
⁹A. Lorke, R. J. Luyken, A. O. Govorov, J. P. Kotthaus, J. M. García, and P. M. Petroff, *Phys. Rev. Lett.* **84**, 2223 (2000).
¹⁰V. Halonen, P. Pietilainen, and T. Chakraborty, *Europhys. Lett.* **33**, 377 (1996).
¹¹Z. Barticevic, M. Pacheco, and A. Latgé, *Phys. Rev. B* **62**, 6963 (2000).
¹²A. Bruno-Alfonso and A. Latgé, *Phys. Rev. B* **61**, 15887 (2000).
¹³Y. Li, H.-M. Lu, O. Voskoboynikov, C. P. Lee, and S. M. Sze, *Surf. Sci.* **532**, 811 (2003).
¹⁴Z. Barticevic, G. Fuster, and M. Pacheco, *Phys. Rev. B* **65**, 193307 (2002).
¹⁵R. J. Warburton, C. Schäfflein, D. Haft, F. Bickel, A. Lorke, K. Karrai, J. M. García, W. Schoenfeld, and P. M. Petroff, *Physica E (Amsterdam)* **9**, 124 (2001).
¹⁶D. Haft, C. Schulhauser, A. O. Govorov, R. J. Warburton, K. Karrai, J. M. García, W. Schoenfeld, and P. M. Petroff, *Physica E (Amsterdam)* **13**, 165 (2002).
¹⁷E. Ribeiro, A. O. Govorov, W. Carvalho, Jr., and G. Medeiros-Ribeiro, *Phys. Rev. Lett.* **92**, 126402 (2004).
¹⁸H. Hu, J.-L. Zhu, D.-J. Li, and J. J. Xiong, *Phys. Rev. B* **63**, 195307 (2001).
¹⁹J. Song and S. E. Ulloa, *Phys. Rev. B* **63**, 125302 (2001).
²⁰J. I. Climente, J. Planelles, and W. Jaskolski, *Phys. Rev. B* **68**, 075307 (2003).
²¹R. A. Römer and M. E. Raikh, *Phys. Rev. B* **62**, 7045 (2000).
²²S. E. Ulloa, A. O. Govorov, A. V. Kalameitsev, R. Warburton, and K. Karrai, *Physica E (Amsterdam)* **12**, 790 (2002).
²³A. O. Govorov, S. E. Ulloa, K. Karrai, and R. J. Warburton, *Phys. Rev. B* **66**, 081309(R) (2002).
²⁴L. G. G. V. Dias da Silva, S. E. Ulloa, and A. O. Govorov, *Phys. Rev. B* **70**, 155318 (2004).
²⁵L. Dias da Silva, S. E. Ulloa, and T. V. Shahbazyan, *Phys. Rev. B* **72**, 125327 (2005).
²⁶A. V. Maslov and D. S. Citrin, *Phys. Rev. B* **67**, 121304(R) (2003).
²⁷K. L. Janssens, B. Partoens, and F. M. Peeters, *Phys. Rev. B* **66**, 075314 (2002); **64**, 155324 (2001).
²⁸L. Jacak, P. Hawrylak, and A. Wójs, *Quantum Dots* (Springer, Berlin, 1998).
²⁹An alternative for having radially polarized excitons is the application of a suitable gate potential at the center of a Type II quantum-dot. The building of a barrier-like structure at the center of the dot will repel the dot-acting particle (an electron in the case of an InP/GaAs Type II quantum-dot) from the central region, resulting in a ring-like structure where the electron and hole move at different radial orbits.
³⁰M. Abramowitz and I. A. Stegun, *Handbook of Mathematical Functions* (Dover, New York, 1972).
³¹C. Kittel, *Introduction to Solid State Physics* (Wiley, New York, 1986).
³²L. D. Landau and E. M. Lifshitz, *Mecánica Cuántica* (Teoría no-relativista) (Editorial Reverté, Barcelona, 1972), p. 85.